Showcasing research from the collaborative efforts of Dr Sujit K. Ghosh's group, Department of Chemistry, IISER Pune (India) and Dr Ravichandar Babarao, Manufacturing, CSIRO, Melbourne (Australia).

Harnessing Lewis acidic open metal sites of metal–organic frameworks: the foremost route to achieve highly selective benzene sorption over cyclohexane

π-Complexation driven Lewis acid–base interactions between open metal sites (OMS) of metal–organic frameworks (MOFs), and π-e^- rich adsorptive benzene (Bz) are utilized to establish M-MOF-74 as the best Bz-selective MOF sorbent; a key advance from the energy-economy standpoint of industrial separation of the azeotropic pair, with very close physical properties.

As featured in:

See Ravichandar Babarao, Sujit K. Ghosh *et al.*, *Chem. Commun.*, 2016, **52**, 8215.

ROYAL SOCIETY OF CHEMISTRY

www.rsc.org/chemcomm

Registered charity number: 207890

ChemComm

COMMUNICATION

View Article Online
View Journal | View Issue

Cite this: *Chem. Commun.*, 2016, 52, 8215

Received 11th April 2016,
Accepted 8th May 2016

DOI: 10.1039/c6cc03015g

www.rsc.org/chemcomm

Harnessing Lewis acidic open metal sites of metal–organic frameworks: the foremost route to achieve highly selective benzene sorption over cyclohexane†

Soumya Mukherjee,[a] Biplab Manna,[a] Aamod V. Desai,[a] Yuefeng Yin,[b] Rajamani Krishna,[c] Ravichandar Babarao*[d] and Sujit K. Ghosh*[a]

π-Complexation triggered Lewis acid–base interactions between open metal sites (OMS) of metal–organic frameworks (MOFs), and π-e$^-$ rich adsorptive benzene (Bz) is exploited to establish M-MOF-74 as the best Bz-selective MOF sorbent, marking the first report of utilizing OMS behind benzene/cyclohexane separation; a key advance from the energy-economy standpoint of industrial separation.

Metal–organic frameworks (MOFs), self-assembled from metal ions/clusters along with multidentate organic linkers,[1] have emerged as one of the most promising new-generation materials, from the standpoint of exhibiting miscellaneous applications.[2] Considering miscellaneous porous adsorbent materials manifested behind the efficient separation of flue gas and industrially relevant hydrocarbons, recent years have witnessed the explicit upsurge of MOFs being established as an inimitably riveting class of functional adsorbents, mainly because of the consummate blend of functionalities, derived from tailor-made strategic design principles.[3]

Focusing on application-frontier, the separation of liquid phase hydrocarbons, particularly those with cognate physical properties and comparable molecular sizes, ubiquitously remain a pressing concern for industrial applications. Under this backdrop, the industrially essential separation of benzene (Bz) and cyclohexane (Cy) is an exigent one. The genesis of such identified intricacy lying behind C_6 hydrocarbon stream separation is the inevitable production of Cy accompanying the catalytic hydrogenation protocol of Bz in the Bz/Cy miscible system, coupled with their markedly similar boiling points (Bz, 353.3 K; Cy, 353.9 K: Table S1, ESI†), related molecular geometry, close Lennard-Jones collision diameters and molecular volumes, in conjunction with low relative volatilities.[4] Conventional fractional distillation methods remaining ineffective, specialized distillation protocols, *viz.* extractive and azeotropic distillations as well as pervaporation, encompass energy-intensive requisites.[5] In contrast to these energy-intensive routes, adsorption-based separations present an energy-efficient alternative, particularly for Bz/Cy mixtures comprising small percentages of Bz, as generally detected in the C_6 flow stream.[6] Focusing on the sorption-targeted porous material domain comprising MOF adsorbents,[7] a ligand prefunctionalization based design principle derived Bz/Cy separation has been only recently revealed,[8] while any other potential alternative rationale is yet to be discovered in the entire MOF regime, particularly with reasonable aqueous stability of the adsorbent.

Notably, the spatial configurational orientations for Bz and Cy involve distinct signatures; aromatic Bz molecules possessing a planar π-cloud entity, in stark contrast to the chair or boat configurations adopted by aliphatic Cy (Fig. S1, ESI†). Herein, we have foreseen this intrinsic disparity to play a key role behind their desired efficient separation (Scheme 1). As a potential strategy, herein, we have envisioned π-complexation triggered facile Lewis acid–base interactions between the OMS-sites of a suitably porous MOF and the targeted adsorptive Bz, to play a pivotal role behind the latter's selective interplay.

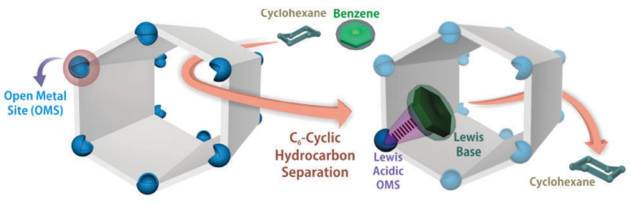

Scheme 1 Schematic representation of the pursued strategy: exploiting Lewis acidic coordinatively unsaturated sites of an OMS-rich MOF platform, to exhibit selective interplay with aromatic, planar Lewis base benzene over its aliphatic, non-planar C_6-analogue cyclohexane.

[a] *Indian Institute of Science Education and Research (IISER), Dr. Homi Bhabha Road, Pashan, Pune 411 008, India. E-mail: sghosh@iiserpune.ac.in*
[b] *Department of Materials Science and Engineering, Monash University, Clayton, Victoria 3800, Australia*
[c] *Van't Hoff Institute for Molecular Sciences, University of Amsterdam, Science Park 904, 1098 XH Amsterdam, The Netherlands*
[d] *Manufacturing, Commonwealth Scientific and Industrial Research Organization (CSIRO), Clayton, Victoria 3168, Australia. E-mail: Ravichandar.Babarao@csiro.au*

† Electronic supplementary information (ESI) available. See DOI: 10.1039/c6cc03015g

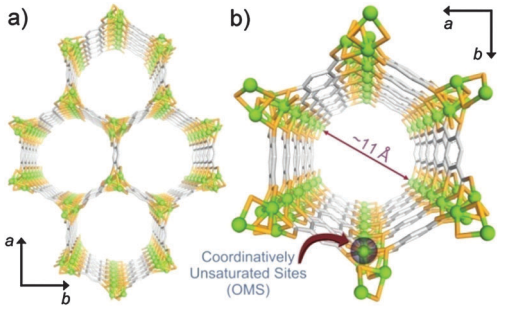

Fig. 1 (a) Perspective representation of the **M-MOF-74** honeycomb 3D architecture presenting 1D hexagonal porous channels along the crystallographic *c*-axis; (b) zoomed-in view of a guest-accessible cylindrical 1D pore (dimension ~11 Å) decorated with cavity-facing OMS centres (green spheres represent the metal centers while oxygen and carbon atoms are shown by orange and grey sticks respectively; H-atoms and non-coordinated solvents have been omitted for clarity).

Keeping in mind the desired amalgamation of the dual facets of OMS-profusion and water-stability, as a first-of-its kind approach, coordinatively unsaturated sites or OMS-rich nanospace of a series of seven isostructural, water-stable metal–organic frameworks (**M-MOF-74**) have been exploited for the purposeful manifestation of selective Bz sorption over its aliphatic analogue, Cy.

Last decade has witnessed the syntheses and subsequent revelation of fascinating sorbent characteristics for a family of isostructural compounds, namely, **M-MOF-74**, alternatively known as M_2(dobdc) (dobdc^{4-} = 2,5-dioxido-1,4-benzenedicarboxylate) or CPO-27-M or M_2(dhtp) (dhtp = 2,5-dihydroxyterephthalate), where M = Mg, Mn, Fe, Co, Ni, Cu, Zn.[9] The 3D honeycomb like network of **M-MOF-74** features helical 1D metal oxide $[O_2M_2](CO_2)_2$ chains which stay connected by the benzene units from dobdc^{4-} linkers, to constitute a hexagonal array of cylindrical channels, with a window size of ~11 Å, propagating across the crystallographic *c*-axis (Fig. 1 and Fig. S2, ESI†); providing an ample guest-accessible BET surface area of ~1500–1600 m^2 g^{-1}.[9c,d,10] The high negative charge residing on the compact dobdc^{4-} ligand leads to a superior metal cation density compared to those of most MOFs with such large pores. The presence of a high concentration of coordinately unsaturated metal cations (~4.5 sites per nm^3),[11a] which pose as the primary interaction sites for adsorptives, has been recently exploited to serve a number of separation purposes for gaseous species.[11] An appropriate activation protocol to this material releases the coordinated water molecules from each metal center, rendering the square pyramidal metal cations with open coordination sites directed into the porous nanospace.[11a] Such presence of extremely reactive metal sites decorating the Connolly surface has posed as an effectual route to infuse framework selectivity for selective guest adsorption, and to enhance the surface packing density of adsorbates.[11b] Therefore, based on exploiting the presumably facile interactions between the π-cloud of adsorptive Bz with the OMS-rich pores of water-stable **M-MOF-74** framework *via* Lewis acid–base type π-complexation interactions,[12] the aforementioned series has been rationally chosen for comprehensive Bz/Cy selectivity analyses.

All seven analogous compounds pertaining to the **M-MOF-74** series (where M = Mg, Mn, Fe, Co, Ni, Cu and Zn) were synthesized.[9e,12c,13] While powder X-ray diffraction (PXRD) analyses confirm the phase purity and isostructural framework nature of the studied guest-free phases (Fig. S3, ESI†), elemental mapping (EDX) for the seven different compounds shows that the respective metals are homogeneously spread out within the areas spanned across by corresponding crystallites (Fig. S4, ESI†).

In order to validate the anticipated selective interaction of adsorbate Bz with **M-MOF-74** compounds, single component vapour sorption experiments for both the solvents Bz and Cy were measured at 298 K for the entire series of MOFs. The contrasting nature of profiles between the said pair of measurements for any of the **M-MOF-74** analogues gets reflected in their differential saturation uptake amounts (**Mn-MOF-74:** 9.38 mmol g^{-1} for Bz, while only 0.25 mmol g^{-1} for Cy) (Fig. 2, Fig. S6–S9 and Table S2, ESI†). All the seven congener MOFs register high uptake amount-indicative Bz sorption profiles of similar nature, with the saturation amounts presenting the following decreasing trend: **Mn-MOF-74** > **Ni-MOF-74** ≈ **Mg-MOF-74** > **Cu-MOF-74** > **Zn-MOF-74** > **Co-MOF-74** > **Fe-MOF-74** (precisely identical order to the decreasing sequence of the ionic potentials of the involved metal ions).[14] Ethyl benzene (dimension-wise larger than Cy) sorption profile for **Co-MOF-74** registered Type-1 isotherm with a high (~4.74 mmol g^{-1}) uptake amount (Fig. S10, ESI†), which served as a testimony of the framework's discriminating interplay with π-rich adsorbates like ethyl benzene, Bz *etc.*, while emphasizing its non-interactive response to aliphatic guests like Cy, albeit the latter's smaller size.[15]

To verify the separation-viability in solution, a representative (**Mg-MOF-74**) was probed by ^{13}C NMR. Solvent vapour of Bz and Cy were separately exposed to the guest-free phase of **Mg-MOF-74** before digesting it in DCl/DMSO-d_6. Only characteristic Bz peaks (δ = 128.3 ppm) could be noted for both Bz and Bz/Cy (1 : 1) vapour exposed phases (Fig. S11 and S12, ESI†), suggesting exclusive interplay with Bz.

To elucidate the different behaviour of Bz adsorption in the **M-MOF-74** analogues, both *NVT* Monte Carlo simulations and density functional theory calculations were further performed. Based on an *NVT* simulated annealing method (details of simulation methods; ESI†), we observe that the Bz molecule explicitly interacts with the Lewis acidic transition metal centers.[16] Further, DFT calculations were performed based on the initial geometry obtained from *NVT* method to determine the binding energies of Bz with the different **M-MOF-74** analogues. Dispersion interactions were included by employing a non-local van der Waals density functional, vdW-DF (see ESI† for more details on the methodology). In all of the **M-MOF-74** analogues, the Bz molecule interacts with the transition metal ions in such a way that the sp^2 hybridized carbon atoms are located close to the metal ions. Fig. 3a and Fig. S14 (ESI†) show the DFT optimized locations of Bz molecule in the different **M-MOF-74** analogues. The binding energies (Table S3, ESI†) calculated based on the vdW-DF functional do not show a large difference amongst the **M-MOF-74** analogues, with **Ni-MOF-74** exhibiting a higher binding energy with Bz molecule followed by **Mn-**, **Zn-**, **Mg-**, **Cu-**, **Co-** and **Fe-MOF-74.** However, Bz has a slightly

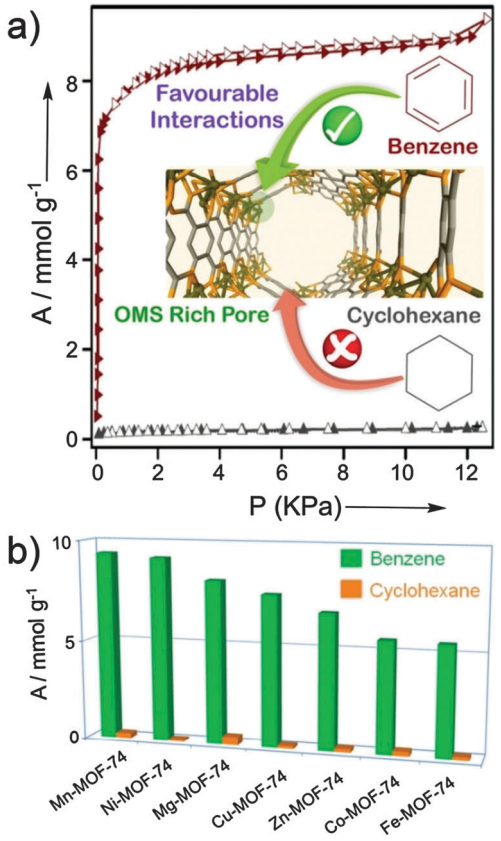

Fig. 2 (a) Contrasting Bz and Cy solvent sorption isotherms for one of the representatives, **Mn-MOF-74**, recorded at 298 K. Filled and open markers denote adsorption and desorption, respectively; (b) Bz and Cy sorption amount uptakes recorded for the entire series of **M-MOF-74** (M = Mg, Mn, Fe, Co, Ni, Cu, Zn) compounds.

weaker interaction with **Co** and **Fe-MOF-74**, as compared to the other **M-MOF-74** analogues. This is somewhat consistent with the trend observed in the sorption isotherms of Bz with different **M-MOF-74** analogues (Fig. 2b and Fig. S8, ESI†).

To quantify the charge transferred from the transition metal ion to adsorbed Bz molecule (π-back-bonding),[17] the magnitude of the net charge transfer using Bader charge population analysis was calculated.[18] Except for **Co** and **Fe-MOF-74**, the net charge transfer from metal ion to Bz follows the order **Mn-MOF-74** (0.0549) > **Ni-MOF-74** (0.0303) > **Mg-MOF-74** (0.0290) > **Cu-MOF-74** (0.0213) > **Zn-MOF-74** (0.0116), which is consistent with the increase in the corresponding ionic potentials of the metal ions. Next, the distribution of charge density difference for adsorption of a single Bz molecule is calculated, considering **Mn-MOF-74** and **Cu-MOF-74** as representatives, as shown in Fig. 3b. The charge density difference ($\Delta\rho$) is calculated by $\Delta\rho = \rho_{(\text{M-MOF-74+Bz})} - \rho_{(\text{M-MOF-74})} - \rho_{\text{Bz}}$, where $\rho_{\text{M-MOF-74+Bz}}$, $\rho_{\text{M-MOF}}$ and ρ_{Bz} are the electronic charge densities of the adsorbed **M-MOF-74**/Bz system, isolated **M-MOF-74** and Bz, respectively. We can observe significant charge redistribution upon Bz adsorption on **M-MOF-74**. As the charge transfer from **M-MOF-74** to Bz increases, the charge redistribution becomes more concentrated around the benzene and metal atoms.

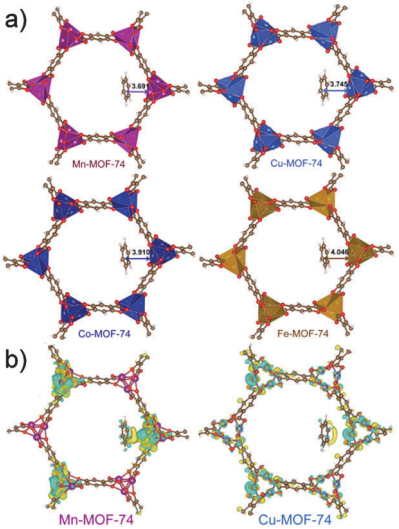

Fig. 3 (a) DFT optimized location of Bz in the different **M-MOF-74** analogues. The distance between the center of the Bz molecule and the transition metal is shown in angstroms; (b) distribution of the charge density difference for single molecular Bz adsorption on **M-MOF-74**. Yellow and cyan isosurfaces indicate the accumulation and depletion electrons at a level of 0.0005 e Å^{-3}, respectively.

Bz/Cy separation efficiency of the **M-MOF-74** series of compounds was evaluated by employing Ideal Adsorbed Solution Theory (IAST) calculations.[19] Unary isotherms for Bz in **M-MOF-74**, were fitted using the three-site Langmuir–Freundlich isotherm model (ESI†); (fit parameters: Table S4, ESI†). For fitting purposes, only the adsorption branches of the isotherms were considered. The unary isotherms for Cy in **M-MOF-74** were fitted using the dual-site Langmuir–Freundlich isotherm model (ESI†); (fit parameters: Table S5, ESI†). In order to demonstrate the goodness of the fitted isotherms, Fig. 4a shows the experimental and fitted data of pure component isotherms for Bz and Cy

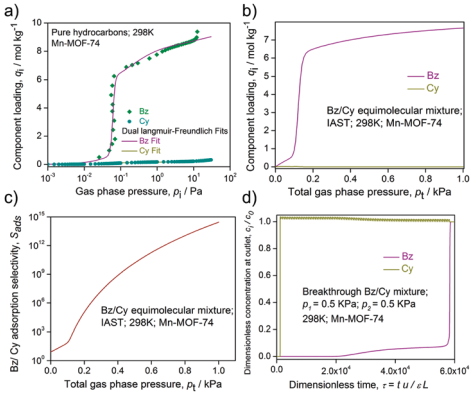

Fig. 4 (a) Comparison of experimental data for pure component isotherms for Bz and Cy in **Mn-MOF-74** with dual-Langmuir–Freundlich fits, which are shown by the continuous solid lines; (b) IAST calculations for Bz uptake capacity for equimolar Bz/Cy mixtures in **Mn-MOF-74**; (c) IAST calculations of adsorption selectivity for equimolar mixtures of Bz/Cy in **Mn-MOF-74**; (d) breakthrough simulations for equimolar Bz/Cy in a fixed bed of **Mn-MOF-74** at 298 K (total pressure at the inlet is 1 kPa).

in **Mn-MOF-74**. Fits for all other **M-MOF-74** materials were also reasonably ideal. Fig. 4b shows IAST calculations for Bz uptake capacity of equimolar Bz/Cy mixtures in **Mn-MOF-74**. We note that for pressures exceeding about 0.2 kPa, the adsorbed phase contains predominantly Bz, while the amount of Cy adsorbed is negligibly small. This indicates excellent separation characteristics. Fig. 4c shows IAST calculations for adsorption selectivity, S_{ads}, for equimolar Bz/Cy mixtures with exceedingly high values in excess of about 10^5 in the case of **Mn-MOF-74**.

In fact, the selectivity values propel this benchmark series of compounds as the top-notch Bz/Cy separating porous MOF materials reported to date.[20] Since the selectivities attained with **Mn-MOF-74** are very high, the separation performance of different **M-MOF-74** materials is simply dictated by the uptake capacity of pure Bz. On the basis of the pure component uptakes of Bz at 12.5 kPa, we conclude that the separation performance of the Bz/Cy mixtures will follow the hierarchy **Mn-MOF-74** > **Mg-MOF-74** ≈ **Ni-MOF-74** > **Cu-MOF-74** > **Zn-MOF-74** > **Co-MOF-74** > **Fe-MOF-74**. The three best MOFs for targeted Bz/Cy separation are **Mn-MOF-74**, **Ni-MOF-74** and **Mg-MOF-74**.

Transient breakthrough simulations,[21] show that strikingly clear separations of equimolar Bz/Cy mixtures are achievable with **Mn-MOF-74** (Fig. 4d). It is evidently noted that Cy gets rejected almost immediately into the bulk fluid phase, and practically no cyclohexane is adsorbed, while precisely contrasting behaviour is manifested for Bz; indicative of fixed bed adsorber based sharp Bz/Cy separation signatures. The video animation (Video S1; ESI†) clearly illustrates that **Mn-MOF-74**: a representative of the **M-MOF-74** series possesses both a significantly higher selectivity and uptake capacity for Bz over Cy.

In summary, as an archetypal modus operandi, the presence of open metal sites acting as Lewis acidic centres could be proficiently exploited behind the realization of highly selective benzene sorption over its aliphatic, azeotropic analogue cyclohexane. This marks the first report of tactically utilizing coordinatively unsaturated sites of a microporous MOF material in course to culminate an excellent selective interplay with the π-cloud of adsorptive benzene. Additional assessments aimed at serving an industrial purpose are presently underway. Such a novel approach might indeed expand the horizons of strategic development lying behind superior functional porous materials of the future, imperative for exhibiting industrially challenging hydrocarbon separation signatures.

INSA (IISER-P/GAP-142/7/2014), IISER Pune and Australian Research Council DECRA fellowship (R. B.) are acknowledged. R. B. acknowledges the computational facilities & services provided through the CSIRO Advanced Scientific Computing, National Computing Infrastructure (NCI) & Pawsey supercomputing facilities.

References

1 S. Kitagawa, R. Kitaura and S.-i. Noro, *Angew. Chem., Int. Ed.*, 2004, **43**, 2334–2375.
2 (*a*) Z. Zhang, Z.-Z. Yao, S. Xiang and B. Chen, *Energy Environ. Sci.*, 2014, **7**, 2868–2899; (*b*) Z. Hu, B. J. Deibert and J. Li, *Chem. Soc. Rev.*, 2014, **43**, 5815–5840.
3 I. Senkovska and S. Kaskel, *Chem. Commun.*, 2014, **50**, 7089–7098.
4 J.-P. Zhang and X.-M. Chen, *J. Am. Chem. Soc.*, 2008, **130**, 6010–6017.
5 (*a*) J. Qin, Q. Ye, X. Xiong and N. Li, *Ind. Eng. Chem. Res.*, 2013, **52**, 10754–10766; (*b*) W. Yin, S. Ding, S. Xia, P. Ma, X. Huang and Z. Zhu, *J. Chem. Eng. Data*, 2010, **55**, 3274–3277.
6 A. Takahashi, F. H. Yang and R. T. Yang, *Ind. Eng. Chem. Res.*, 2000, **39**, 3856–3867.
7 S.-C. Xiang, Z. Zhang, C.-G. Zhao, K. Hong, X. Zhao, D.-R. Ding, M.-H. Xie, C.-D. Wu, M. C. Das, R. Gill, K. M. Thomas and B. Chen, *Nat. Commun.*, 2011, **2**, 204.
8 (*a*) S. Shimomura, S. Horike, R. Matsuda and S. Kitagawa, *J. Am. Chem. Soc.*, 2007, **129**, 10990–10991; (*b*) S. Shimomura, R. Matsuda and S. Kitagawa, *Chem. Mater.*, 2010, **22**, 4129.
9 (*a*) N. L. Rosi, J. Kim, M. Eddaoudi, B. Chen, M. O'Keeffe and O. M. Yaghi, *J. Am. Chem. Soc.*, 2005, **127**, 1504–1518; (*b*) P. D. C. Dietzel, Y. Morita, R. Blom and H. Fjellvåg, *Angew. Chem., Int. Ed.*, 2005, **44**, 6354–6358; (*c*) P. D. C. Dietzel, R. E. Johnsen, R. Blom and H. Fjellvåg, *Chem. – Eur. J.*, 2008, **14**, 2389–2397; (*d*) S. R. Caskey, A. G. Wong-Foy and A. J. Matzger, *J. Am. Chem. Soc.*, 2008, **130**, 10870–10871; (*e*) T. Grant Glover, G. W. Peterson, B. J. Schindler, D. Britt and O. M. Yaghi, *Chem. Eng. Sci.*, 2011, **66**, 163–170; (*f*) W. L. Queen, M. R. Hudson, E. D. Bloch, J. A. Mason, M. I. Gonzalez, J. S. Lee, D. Gygi, J. D. Howe, K. Lee, T. A. Darwish, M. James, V. K. Peterson, S. J. Teat, B. Smit, J. B. Neaton, J. R. Long and C. M. Brown, *Chem. Sci.*, 2014, **5**, 4569–4581.
10 E. D. Bloch, W. L. Queen, R. Krishna, J. M. Zadrozny, C. M. Brown and J. R. Long, *Science*, 2012, **335**, 1606–1610.
11 (*a*) D. Britt, H. Furukawa, B. Wang, T. G. Glover and O. M. Yaghi, *Proc. Natl. Acad. Sci. U. S. A.*, 2009, **106**, 20637–20640; (*b*) Y. He, R. Krishna and B. Chen, *Energy Environ. Sci.*, 2012, **5**, 9107–9120.
12 (*a*) X.-J. Hou, P. He, H. Li and X. Wang, *J. Phys. Chem. C*, 2013, **117**, 2824–2834; (*b*) H. Kim, J. Park and Y. Jung, *Phys. Chem. Chem. Phys.*, 2013, **15**, 19644–19650; (*c*) G. Calleja, R. Sanz, G. Orcajo, D. Briones, P. Leo and F. Martínez, *Catal. Today*, 2014, **227**, 130–137.
13 (*a*) E. D. Bloch, L. J. Murray, W. L. Queen, S. Chavan, S. N. Maximoff, J. P. Bigi, R. Krishna, V. K. Peterson, F. Grandjean, G. J. Long, B. Smit, S. Bordiga, C. M. Brown and J. R. Long, *J. Am. Chem. Soc.*, 2011, **133**, 14814–14822; (*b*) A. F. Cozzolino, C. K. Brozek, R. D. Palmer, J. Yano, M. Li and M. Dincă, *J. Am. Chem. Soc.*, 2014, **136**, 3334–3337.
14 (*a*) F. A. Cotton, G. Wilkinson and P. L. Gaus, *Basic Inorganic Chemistry*, John Wiley and Sons, Inc., 3rd edn, 1994; (*b*) https://www.ionicviper.org/class-activity/polarizing-power-cations.
15 C. E. Webster, R. S. Drago and M. C. Zerner, *J. Am. Chem. Soc.*, 1998, **120**, 5509–5516.
16 (*a*) A. S. Mahadevi and G. N. Sastry, *Chem. Rev.*, 2013, **113**, 2100–2138; (*b*) D. A. Dougherty, *Acc. Chem. Res.*, 2013, **46**, 885–893.
17 (*a*) K. Lee, J. D. Howe, L.-C. Lin, B. Smit and J. B. Neaton, *Chem. Mater.*, 2015, **27**, 668–678; (*b*) H.-B. Yi, H. M. Lee and K. S. Kim, *J. Chem. Theory Comput.*, 2009, **5**, 1709–1717.
18 G. Henkelman, A. Arnaldsson and H. Jónsson, *Comput. Mater. Sci.*, 2006, **36**, 354–360.
19 A. L. Myers and J. M. Prausnitz, *AIChE J.*, 1965, **11**, 121–127.
20 B. Manna, S. Mukherjee, A. V. Desai, S. Sharma, R. Krishna and S. K. Ghosh, *Chem. Commun.*, 2015, **51**, 15386–15389, and references therein.
21 R. Krishna, *RSC Adv.*, 2015, **5**, 52269–52295.

Supporting Information

Harnessing Lewis Acidic Open Metal Sites of Metal-organic Frameworks: Foremost Route to Achieve Highly Selective Benzene Sorption over Cyclohexane

Soumya Mukherjee,[a] Biplab Manna,[a] Aamod V. Desai,[a] Yuefeng Yin,[b] Rajamani Krishna,[c] Ravichandar Babarao,*[d] and Sujit K. Ghosh*[a]

[a]Indian Institute of Science Education and Research (IISER), Dr. Homi Bhabha Road, Pashan, Pune-411008, India.

Fax: +91 20 2590 8186. E-mail: sghosh@iiserpune.ac.in

[b]Department of Materials Science and Engineering, Monash University, Clayton, Victoria 3800, Australia.

[c]Van 't Hoff Institute for Molecular Sciences, University of Amsterdam, Science Park 904, 1098 XH Amsterdam, The Netherlands.

[d]Manufacturing, Commonwealth Scientific and Industrial Research Organization (CSIRO), Clayton, Victoria 3168, Australia. E-mail: Ravichandar.Babarao@csiro.au

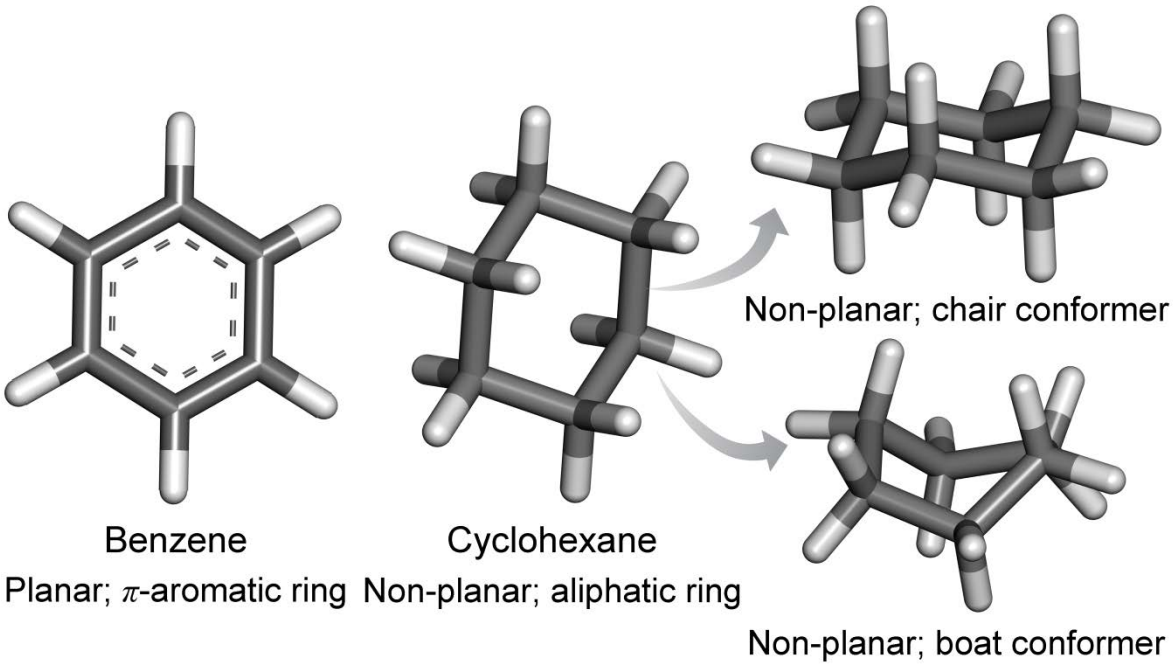

Figure S1: General conformations of planar aromatic π-ring Benzene (Bz) (left) and non-planar aliphatic congener Cyclohexane (Cy) (middle): chair (top right) and boat (bottom right) conformers.

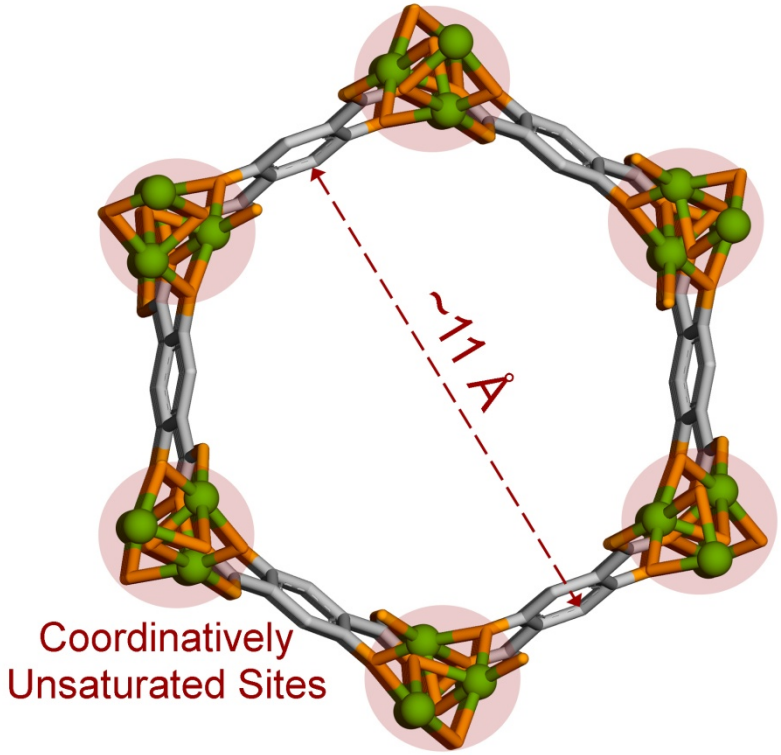

Figure S2: Orthographic view of a single pore along crystallographic *c*-axis; the pore being decorated with open metal sites or coordinatively unsaturated metal centres, with a window size ~ 11 Å.

Table S1. Physical Properties of C_6 adsorptive species.

Dimensions of Adsorptive molecules (Å)[S1] (each atom surrounded by a van der Waals sphere)						Boiling and Freezing Points		Conformers
Dimensional Closeness								
	x	***y***	**z**	**MIN-1**	**MIN-2**	**B.P.**	**F.P.**	**Type(s)**
Bz	6.628	7.337	3.277	3.277	6.628	353.3 K	278.7 K	Planar
Cy	7.168	6.580	4.982	4.982	6.580	353.9 K	279.6 K	Non-planar: Boat and Chair

MIN-1: Size of the adsorptive in the minimum dimension.
MIN-2: Second minimum dimension for molecular orientations that enable a molecule to enter the channel.

Table S2. Comparative analysis of the saturation uptake amounts recorded for the C_6-hydrocarbon pair Benzene and Cyclohexane in case of all the seven **M-MOF-74** compounds.

Compound	**Bz Saturation Uptake Amounts (12.5 KPa) (mmolg^{-1})**	**Cy Saturation Uptake Amounts (12.5 KPa) (mmolg^{-1})**
Mg-MOF-74	8.15	0.40
Mn-MOF-74	9.38	0.25
Fe-MOF-74	5.50	0.15
Co-MOF-74	5.57	0.23
Ni-MOF-74	9.19	0.09
Cu-MOF-74	7.55	0.13
Zn-MOF-74	6.76	0.17

Experimental Section:

Materials and measurements:

Unless otherwise noted, all the reagents and solvents were commercially available and used without further purification. Physical measurements:

Powder X-ray diffraction (PXRD) patterns were measured on Bruker D8 Advanced X-Ray diffractometer at room temperature using Cu-Kα radiation (λ= 1.5406 Å) with a scan speed of 0.5° min^{-1} and a step size of 0.01° in 2 *theta*. Thermogravimetric analysis was recorded on Perkin-Elmer STA 6000, TGA analyzer under N_2 atmosphere with heating rate of 10° C/min.

Low-Pressure Solvent Sorption Measurements

Low-pressure solvent (Bz and Cy) sorption measurements were performed using BelAqua (Bel Japan). As-synthesized **M-MOF-74** compounds (as prepared by the reported protocols) [9e, 12c,13] were exchanged thrice each day over a period of seven days with fresh batches of dry methanol, before heating each at 210 °C under vacuum to end up with guest-free, activated crystalline phases, suitable for sorption analysis.

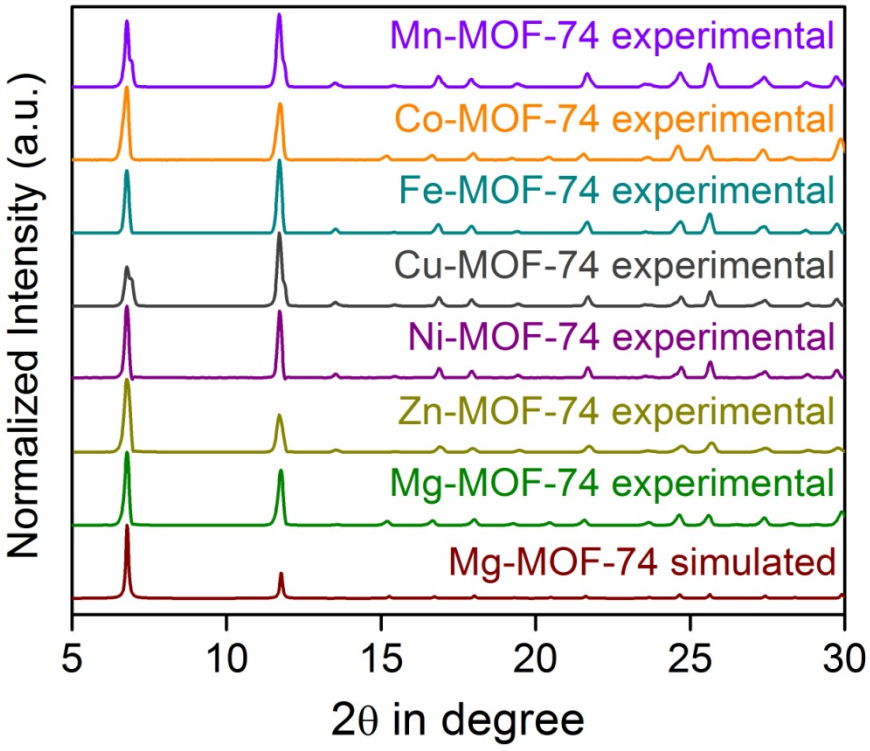

Figure S3: Similar experimental PXRD profiles for all the seven **M-MOF-74** analogous compounds, plotted relative to the simulated pattern of **Mg-MOF-74**.

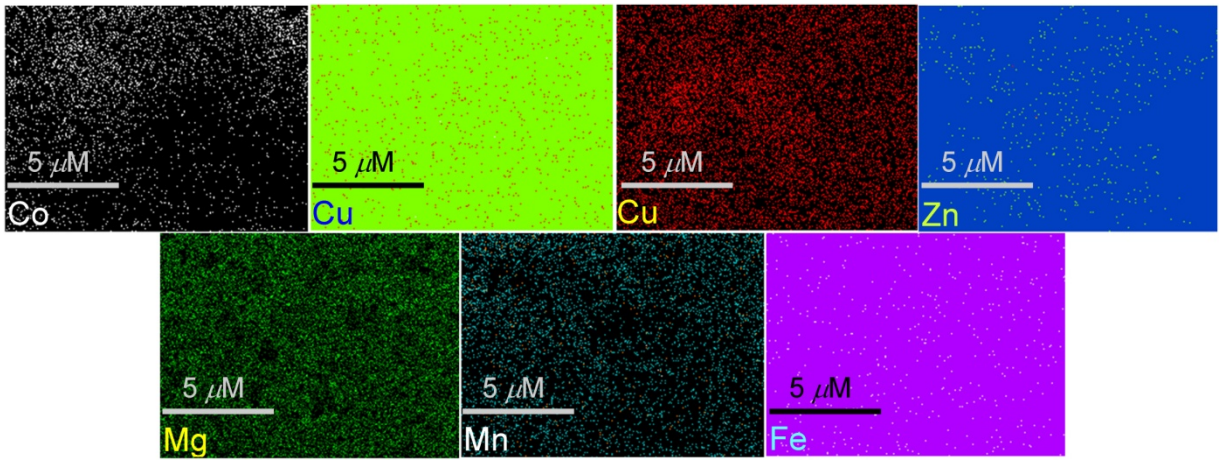

Figure S4: Elemental mapping (EDX) images of the different metals in cases of the seven **M-MOF-74** compounds.

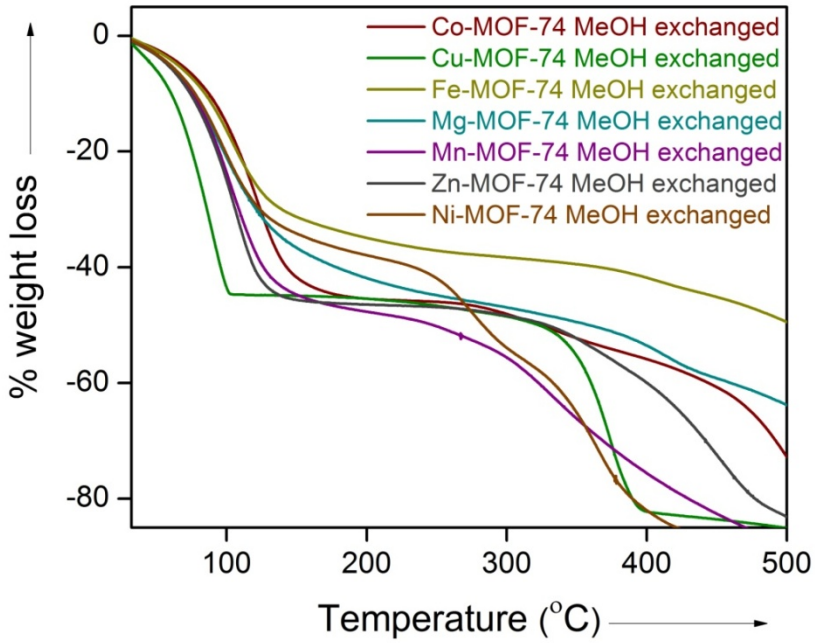

Figure S5: Thermogravimetric analysis profiles for the MeOH-exchanged phases of **M-MOF-74** compounds.

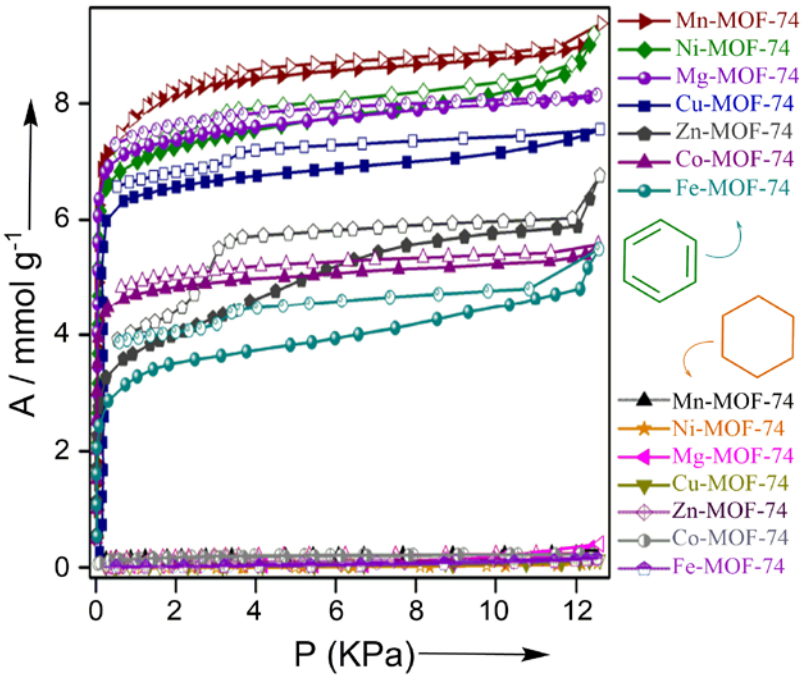

Figure S6: Single component solvent sorption isotherms (Bz and Cy) for the series of **M-MOF-74** (M= Mg, Mn, Fe, Co, Ni, Cu, Zn) compounds recorded at 298 K (in terms of mmol per g versus P in KPa). Filled and open markers denote adsorption and desorption, respectively.

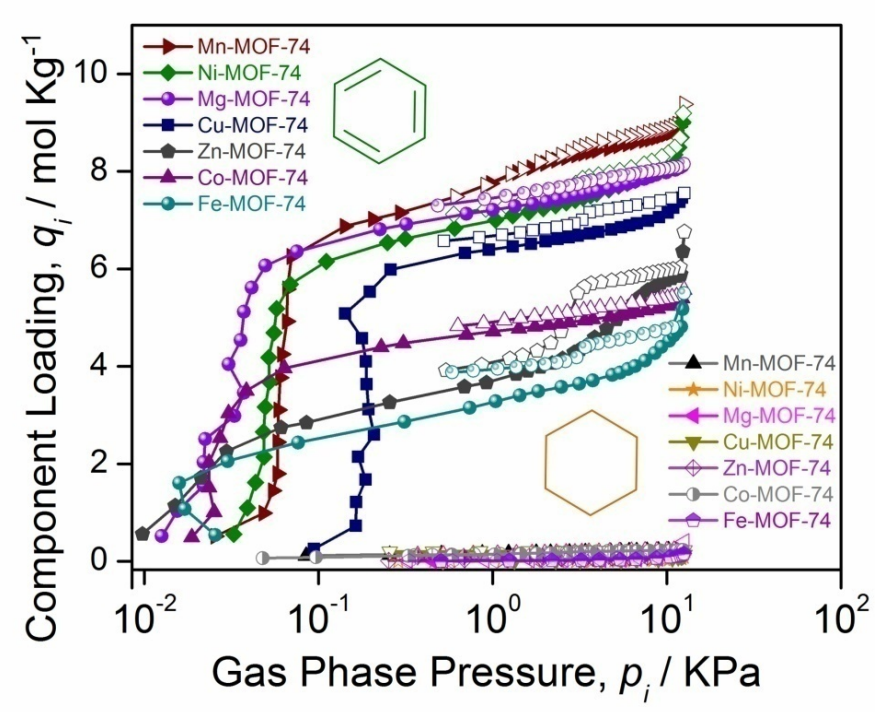

Figure S7: Comparison of unary benzene isotherms in **M-MOF-74** at 298 K.

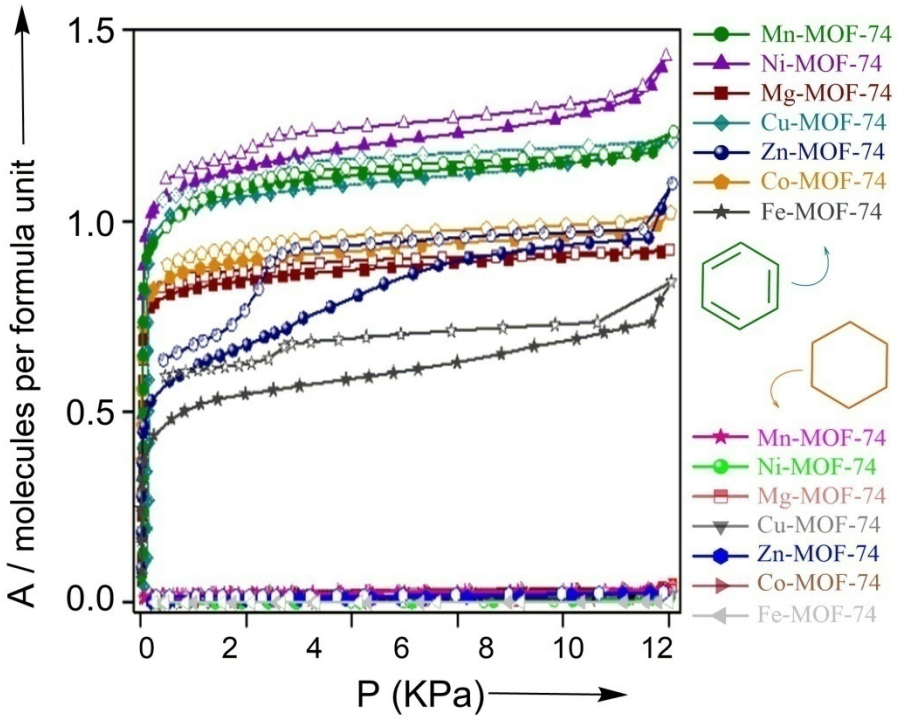

Figure S8: Single component solvent sorption isotherms (Bz and Cy) for the series of **M-MOF-74** (M= Mg, Mn, Fe, Co, Ni, Cu, Zn) compounds recorded at 298 K (in terms of molecules per formula unit versus P in KPa). Filled and open markers denote adsorption and desorption, respectively.

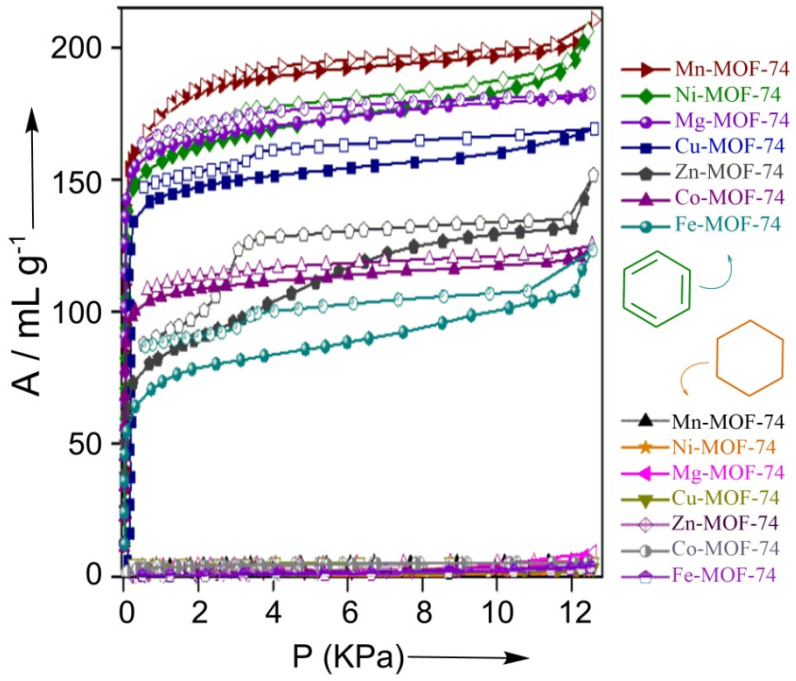

Figure S9: Single component solvent sorption isotherms (Bz and Cy) for the series of **M-MOF-74** (M= Mg, Mn, Fe, Co, Ni, Cu, Zn) compounds recorded at 298 K (in terms of mL per gram versus P in KPa). Filled and open markers denote adsorption and desorption, respectively.

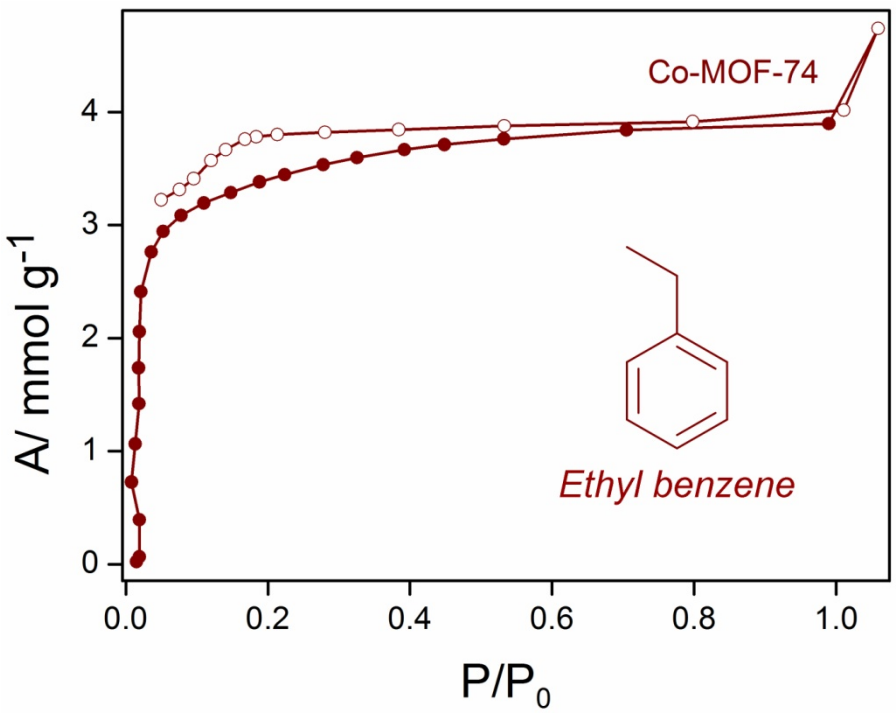

Figure S10: Single component ethyl benzene sorption isotherm for **Co-MOF-74** (one representative among the series of **M-MOF-74**), recorded at 298 K (in terms of mmol per gram versus P/P_0). Filled and open markers denote adsorption and desorption, respectively.

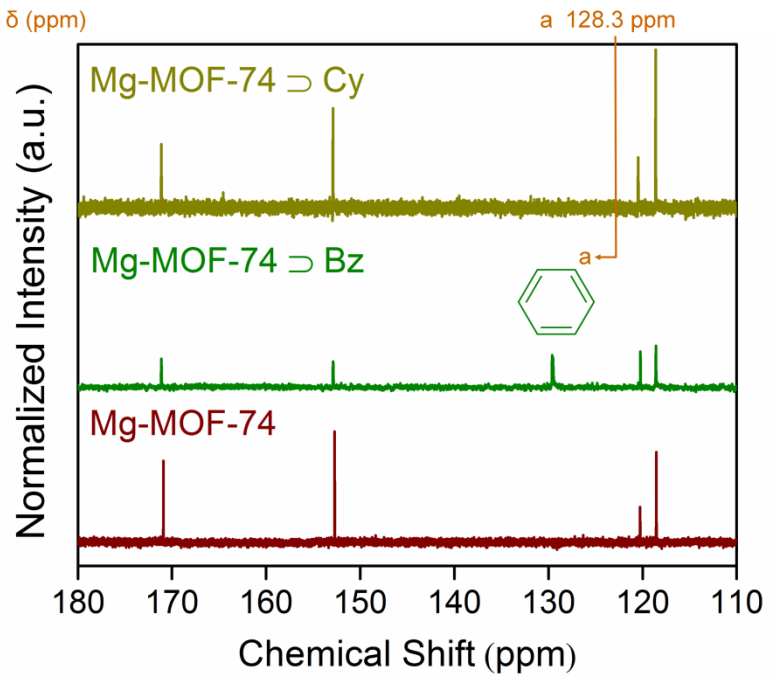

Figure S11: ^{13}C NMR spectra for Bz and Cy vapor-exposed phases of compound **Mg-MOF-74**, as compared to the desolvated phase itself.

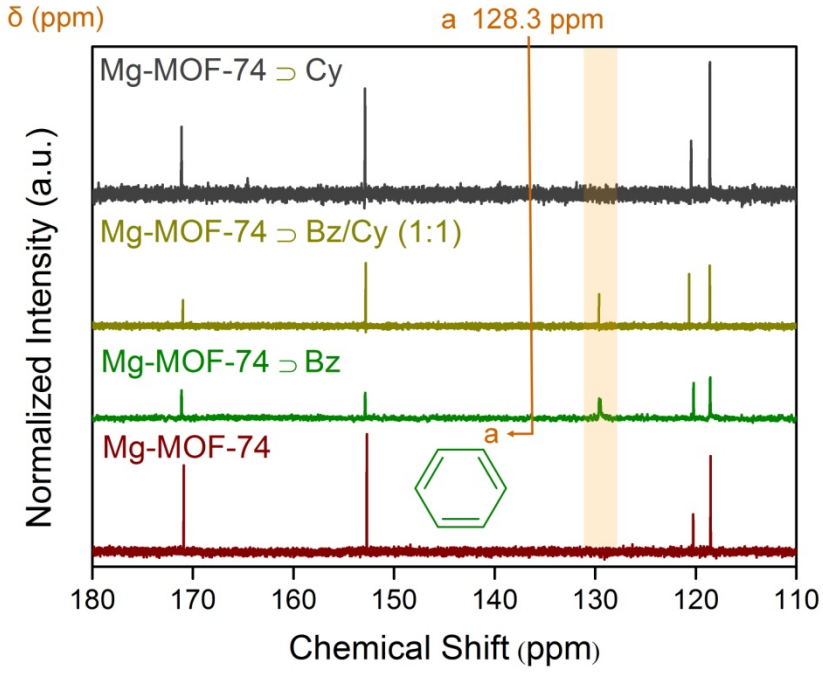

Figure S12: ^{13}C NMR spectra for 1:1 equimolar mixtures of Bz/Cy exposed phase of **Mg-MOF-74**, as compared to the Bz and Cy vapor-exposed phases of compound **Mg-MOF-74**, and the one for desolvated phase itself.

Simulation Methodology

NVT simulation:

The initial geometry of benzene molecule in **M-MOF-74** (M – Mg, Mn, Fe, Co, Cu, Zn and Ni) was estimated based on simulated annealing method using classical force field as implemented in sorption module in *Materials Studio*.[S2] The crystal structures for the **M-MOF-74** were taken from the literature.[S3-S5] The configurational-bias algorithm was used rather than the conventional *Metropolis* technique, which is prohibitively expensive in sampling the phase space of big molecules. In configurational-bias algorithm, a molecule is grown atom-by-atom biasing energetically favorable configurations while avoiding overlap with other atoms.[S6, S7] The simulation box contained super cell and the periodic boundary conditions were exerted in all three dimensions. In the simulated annealing method, the temperature is lowered in succession allowing the gas molecule to reach a desirable configuration based on different moves such as rotate, translate and re-position with preset probabilities of occurrence. This process of heating and cooling the system was repeated in several heating cycles to find the local minima. Forty heating cycles were performed where the maximum temperature and the final temperature were 10^5 K and 100 K, respectively. The NVT ensemble process consisted of 10^7 equilibration steps followed by 10^7 production steps, with the properties calculated from the latter steps. The LJ interactions were evaluated using a spherical cutoff of 12.5 Å and the Coulombic interactions were calculated using the Ewald summation with a precision of 10^{-5}. Five types of trial moves were randomly attempted in the MC simulation, namely, translation, rotation, twist, regrowth, and exchange including creation and deletion with equal probability.

The long-range Coulombic interactions are computed with a Ewald summation technique using point charges assigned to both the framework atoms and the guest molecules. The point charges assigned to the framework atoms are adopted from earlier work reported in the literature.[S8, S9] Dispersion interaction energies are computed from a Lennard-Jones potential form with parameters from the universal force field (UFF)[S10] for both the framework atom and guest molecule. The Lorentz− Berthelot mixing rule is used for the pairwise interaction parameters between two different atomic species.

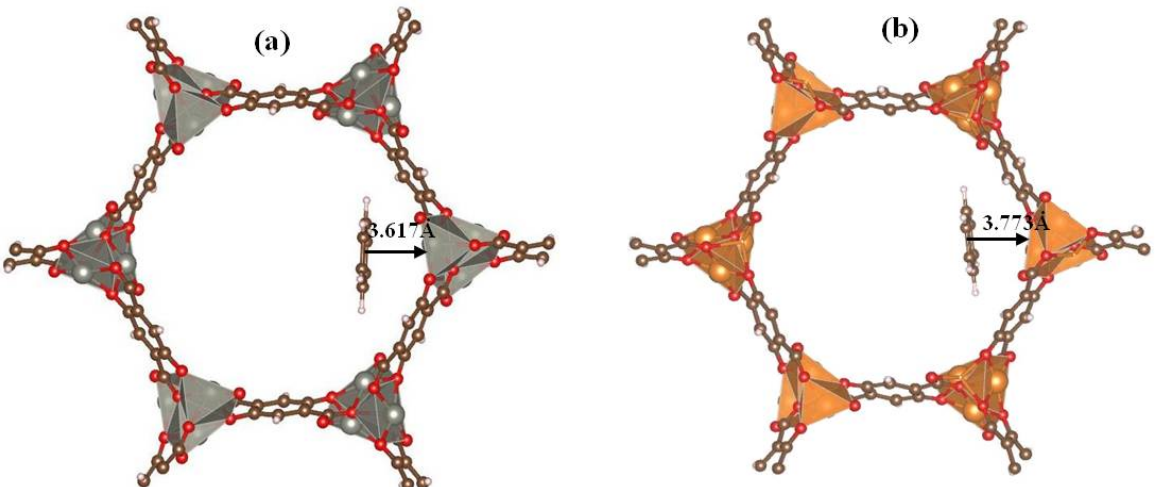

Figure S13. Location of benzene in (a) **Zn-MOF-74**, and (b) **Mg-MOF-74** identified from NVT simulated annealing method. For clarity the hexagonal cell is cleaved from the supercell to represent the location of guest molecule. The distance between the centriod of benzene and metal ion is shown in angstroms. Similarly for other **M-MOF-74** analogues, we obtained the lowest energy configuration of benzene using simulated annealing method.

Density Functional Theory (DFT) calculations

Static binding energies for benzene molecule at 0 K were calculated using the van der Waals density functional (vdW-DF) method.[S11] All calculations were performed using Vienna *ab initio* simulation package (VASP)[S12, S13] with a plane-wave energy cut-off of 860 eV and k-point sampling at the gamma-point. Hubbard U corrections are not included in the calculation. The interactions between core and valence electrons were described by the projector-augmented-wave (PAW) method[S14] and revPBE[S15] was used to parameterize the exchange-correlation functional. Recent studies revealed that the binding energy and the distance between benzene and transition metal surfaces obtained from vdW-DF and vDW-DF2 are more or less similar, but differ significantly from those of the opt-type van der Waals functionals.[S16] However, the different functional used in vdW-DF are not tested in this work as no experimental heat of adsorption is available to validate the methods.

The initial location of single benzene molecule in the periodic cell was obtained from the classical simulated annealing technique as described in the NVT simulation section. During relaxation, both the lattice vectors and the atomic positions are simultaneously optimized. The atomic positions and the lattice vectors are optimized until the residual forces are smaller

than 0.01 eV/Å. Static binding energies (ΔE) at 0 K were calculated using the following expression;

$$\Delta E = E_{MOF+benzene} - E_{MOF} - E_{benzene}$$

where E_x refers, respectively, to the total energies of the MOF + benzene complex, the MOF alone, and benzene molecule.

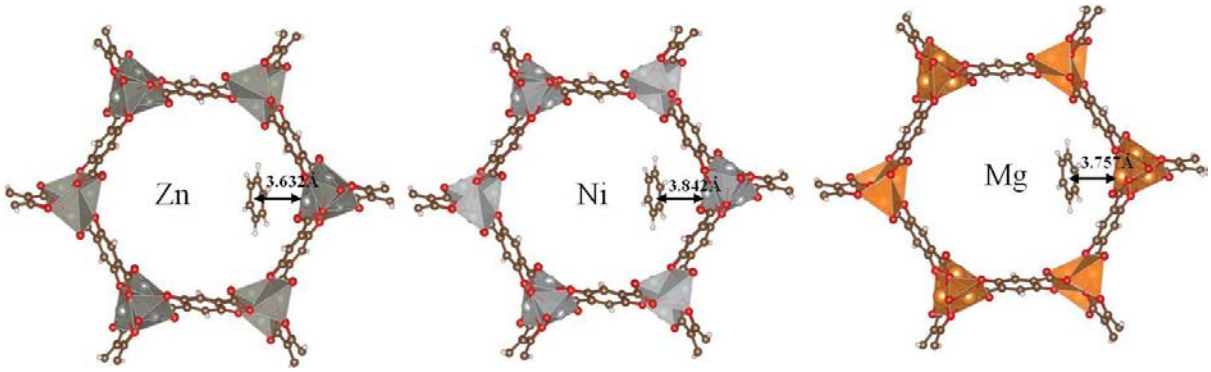

Figure S14. Optimized location of benzene based on van der Waals density functional in **M-MOF-74** analogues. The distance between the centre of the benzene molecule and the transition metals are shown in angstroms.

Table S3. Vdw-DF calculated adsorption energies (in kJ/mol) of a single benzene molecule in **M-MOF-74** analogues.

M-MOF-74	ΔE^a
Ni-MOF-74	-71.77
Mn-MOF-74	-68.09
Zn-MOF-74	-68.95
Mg-MOF-74	-67.57
Cu-MOF-74	-66.86
Co-MOF-74	-65.49
Fe-MOF-74	-65.31

[a] ΔE refers to the static 0 K adsorption energy.

Table S4. Three-site Langmuir-Freundlich parameters for adsorption of benzene in **M-MOF-74** at 298 K.

$$q = q_{A,sat}\frac{b_A p^{\nu_A}}{1+b_A p^{\nu_A}} + q_{B,sat}\frac{b_B p^{\nu_B}}{1+b_B p^{\nu_B}} + q_{C,sat}\frac{b_C p^{\nu_C}}{1+b_C p^{\nu_C}}$$

	Site A			**Site B**			**Site C**		
	$q_{A,sat}$ mol kg^{-1}	b_A Pa$^{-\nu_A}$	ν_A dimensionless	$q_{B,sat}$ mol kg^{-1}	b_B Pa$^{-\nu_B}$	ν_B dimensionless	$Q_{C,sat}$ mol kg^{-1}	b_C Pa$^{-\nu_C}$	ν_C dimensionless
Mn	1	0.00004	1	5.5	1E-25	14	3	0.005	1
Ni	0.5	0.00004	1	4.65	1.2E-25	15	3.2	0.005	1
Mg	0.4	0.00004	1	5.5	1.2E-25	18	2.3	0.005	1
Cu	0.4	0.00001	1	5.1	1E-33	14.5	2.2	0.001	1
Zn	2.3	0.00001	1	2.5	1E-07	6	2.5	0.001	1
Co	0.4	0.00004	1	3.5	1.2E-25	18	1.5	0.005	1
Fe	2.2	0.00001	1	2.3	1E-07	6	2	0.001	1

For a binary mixture the adsorption selectivity is defined as follows

$$S_{ads} = \frac{q_1/q_2}{p_1/p_2}$$

Table S5. Two-site Langmuir-Freundlich parameters for adsorption of cyclohexane in **M-MOF-74** at 298 K.

$$q = q_{A,sat}\frac{b_A p^{\nu_A}}{1+b_A p^{\nu_A}} + q_{B,sat}\frac{b_B p^{\nu_B}}{1+b_B p^{\nu_B}}$$

	Site A			**Site B**		
	$q_{A,sat}$ mol kg^{-1}	b_A Pa$^{-\nu_A}$	ν_A dimensionless	$q_{B,sat}$ mol kg^{-1}	b_B Pa$^{-\nu_B}$	ν_B dimensionless
Mn	0.19	0.01	1	0.3	2E-08	1.7
Ni	0.7	0.000001	1	0.2	1E-29	7
Mg	1	0.00001	1	1	1E-46	11
Cu	5	0.000001	1	1	1E-34	8
Zn	0.15	0.0002	1	0.1	0.00004	1
Co	0.14	0.01	1	0.1	0.0002	1
Fe	5	0.000001	1	1	1E-34	8

Notation

b_A	dual-Langmuir-Freundlich constant for species *i* at adsorption site A, $Pa^{-\nu_i}$
b_B	dual-Langmuir-Freundlich constant for species *i* at adsorption site B, $Pa^{-\nu_i}$
c_i	molar concentration of species *i* in fluid mixture, mol m^{-3}
c_{i0}	molar concentration of species *i* in fluid mixture at inlet to adsorber, mol m^{-3}
L	length of packed bed adsorber, m
n	number of species in the mixture, dimensionless
p_i	partial pressure of species *i* in mixture, Pa
p_t	total system pressure, Pa
q_i	component molar loading of species *i*, mol kg^{-1}
$q_{i,sat}$	molar loading of species *i* at saturation, mol kg^{-1}
q_t	total molar loading in mixture, mol kg^{-1}
$q_{sat,A}$	saturation loading of site A, mol kg^{-1}
$q_{sat,B}$	saturation loading of site B, mol kg^{-1}
t	time, s
T	absolute temperature, K
u	superficial gas velocity in packed bed, m s^{-1}
v	interstitial gas velocity in packed bed, m s^{-1}

Greek letters

ε	voidage of packed bed, dimensionless
ν	exponent in dual-Langmuir-Freundlich isotherm, dimensionless
θ_t	fractional occupancy within the pores, dimensionless
ρ	framework density, kg m^{-3}
τ	time, dimensionless

Subscripts

i	referring to component *i*
A	referring to site A
B	referring to site B
t	referring to total mixture

References:

S1. C. E. Webster, R. S. Drago, and M. C. Zerner, *J. Am. Chem. Soc.*1998, **120**, 5509-5516.

S2. *Materials Studio, 7.0 ed.;*, Accelrys, San Diego, 2012.

S3. W. Zhou, H. Wu, and T. Yildirim, *J. Am. Chem. Soc.* 2008, **130**, 15268-15269.

S4. R. Sanz, F. Martinez, G. Orcajo, L. Wojtas, and D. Briones, *Dalton Trans.* **2013**, *42*, 2392-2398.

S5. D. J. Xiao, E. D. Bloch, J. A. Mason, W. L. Queen, M. R. Hudson, N. Planas, J. Borycz, A. L. Dzubak, P. Verma, K. Lee, F. Bonino, V. Crocella, J. Yano, S. Bordiga, D. G. Truhlar, L. Gagliardi, C. M. Brown, and J. R. Long, *Nat. Chem.* 2014, **6**, 590-595.

S6. D. Frenkel, G. Mooij, and B. Smit, *J. Phys.: Condensed Matter* 1992, **4**, 3053-3076.

S7. J. I. Siepmann, and D. Frenkel, *Mol. Phys.* 1992, **75**, 59-70.

S8. J. Borycz, L.-C. Lin, E. D. Bloch, J. Kim, A. L. Dzubak, R. Maurice, D. Semrouni, K. Lee, B. Smit, and L. Gagliardi, *J. Phys. Chem. C* 2014, **118**, 12230-12240.

S9. T. Pham, K. A. Forrest, J. Eckert, and B. Space, *Cryst. Growth Des.* 2016, **16**, 867-874.

S10. A. K. Rappe, C. J. Casewit, K. S. Colwell, W. A. Goddard, and W. M. Skiff, *J. Am. Chem. Soc.* 1992, **114**, 10024-10035.

S11. A. Puzder, M. Dion, and D. C. Langreth, *J. Chem. Phys.* 2006, **124**.

S12. G. Kresse, and J. Hafner, *Phys. Rev. B* 1993, **48**, 13115-13118.

S13. G. Kresse, and J. Furthmuller, *Comput. Mater. Sci.* 1996, **6**, 15-50.

S14. G. Kresse, and D. Joubert, *Phys. Rev. B* 1999, **59**, 1758-1775.

S15. M. Dion, H. Rydberg, E. Schroder, D. C. Langreth, and B. I. Lundqvist, *Phys. Rev. Lett.* 2004, **92**.

S16. J. Klimes, D. R. Bowler, and A. Michaelides, *J. Phys.: Condens. Matter* 2010, **22**.